AIAA JOURNAL
Vol. 39, No. 7, July 2001

Large-Eddy Simulation of a Supersonic Boundary Layer Using an Unstructured Grid

Gerald Urbin* and Doyle Knight†
Rutgers University, Piscataway, New Jersey 08854

A Mach 3 adiabatic flat plate turbulent boundary layer is studied using large-eddy simulation (LES). The filtered compressible Navier–Stokes equations are solved on a three-dimensional unstructured grid of tetrahedral cells. A compressible extension of the rescaling–reintroducing process of Lund et al. (Lund, T., Wu, X., and Squires, K., "Generation of Turbulent Inflow Data for Spatially-Developing Boundary Layer Simulations," *Journal of Computational Physics*, Vol. 140, No. 2, 1998, pp. 233–258) is developed to generate the inflow conditions. The effect of the subgrid-scale motion is incorporated using two approaches, namely, monotone integrated LES (MILES) and the Smagorinsky subgrid-scale model. A detailed grid refinement study is performed. The statistical predictions (friction velocity, adiabatic wall temperature, mean velocity profile, normal Reynolds stress, and Reynolds shear stress) obtained from MILES are in close agreement with experimental data and direct numerical simulation. The results indicate that the subgrid-scale effects can be adequately modeled using MILES without the need for the Smagorinsky model.

Introduction

MOST studies using large-eddy simulation (LES) have mainly focused on incompressible and subsonic flows.[1] In addition, most LES codes employ structured meshes in the context of finite difference or spectral methods.[2] There is a significant need for research in compressible LES for application to practical aeronautical configurations.[3] Unstructured grids are commonly employed in simulation of complex aeronautical systems because they can be generated substantially faster than block-structured (fitted or overset) grids.[4]

This paper presents three contributions to compressible LES. First, we present a three-dimensional fully unstructured grid LES algorithm for compressible turbulent flow. The algorithm is second- or third-order accurate in space and second-order accurate in time. It has previously been validated for two subsonic flows, namely, the decay of isotropic turbulence[5] and subsonic channel flow.[6] In this paper, we validate the algorithm for a Mach 3 supersonic turbulent boundary layer by comparison with experimental data. Second, we demonstrate the accuracy of the monotone integrated LES (MILES) approach for a supersonic boundary layer. The MILES approach, described by Boris et al.[7] and Oran and Boris,[8] implicitly models the subgrid-scale stresses and heat transfer through the numerical algorithm. MILES is particulary well suited for low-order accurate but not overly dissipative schemes. It has been previously validated for a wide range of free shear flows.[7–11] We present herein the first validation of the MILES methodology for a supersonic turbulent boundary layer. Third, we present a method for defining the unsteady inflow boundary condition in a supersonic flat plate turbulent boundary layer based on a rescaling of the flow at a downstream location and reintroduction at the inflow boundary. Our method represents the compressible extension of the technique of Lund et al.,[12] which was developed for incompressible flows.

Previous LES studies of compressible flow can be divided into two categories, namely, those which employed a subgrid scale model and those based on MILES. Examples of the former category include Erlebacher et al.,[13] Spyropoulos and Blaisdell,[14] Jansen,[15] Ducros et al.,[16] and Haworth and Jansen.[17] Except for Haworth and Jansen, all of these simulations are based on the traditionally high-order accurate schemes, which are not well suited to fully unstructured grids. Haworth and Jansen use the recent NO-UTOPIA second-order accurate spatial scheme for unstructured meshes to test different models (constant coefficient Smagorinsky model, dynamic Smagorinsky model, and Lagrangian dynamic Smagorinsky model). In some cases the models do not demonstrate any advantage compared to the abscence of any explicit subgrid-scale model. Examples of the second category include Boris et al.,[7] Fureby and Grinstein,[9] Grinstein,[10] Oran and Boris,[8] and Porter et al.,[11] all of which employed second-order or third-order accurate spatial schemes.

Both LES and direct numerical simulation (DNS) studies of compressible turbulent boundary layers are scarce. DNS of a spatially developing boundary layer, that is, the natural configuration, requires a large number of grid points, and therefore, typically only the earliest stage of transition to turbulence is simulated.[18–20] Various methods have been developed to approximately transform the spatially developing boundary layer to a temporally developing configuration to reduce the computational effort and/or increase the maximum Reynolds number.[12,21–24] Nevertheless these simulations are restricted to relatively low Reynolds numbers. LES studies of boundary layers have been able to reach higher-Reynolds-number flows[16,25] than DNS. Nevertheless simulating a spatially developing turbulent boundary layer from the initial laminar state through transition to a fully developed turbulent state is still very computationally intensive. The rescaling–reintroduction methodology described in this paper substantially reduces the computational time.

LES Methodology

In this section we summarize the LES methodology, including the governing equations, subgrid-scale (SGS) model, and numerical implementation. Additional details (including information on parallelization) are presented by Knight et al.[5] and Okong'o and Knight.[6]

Governing Equations

The governing equations are the three-dimensional filtered Navier–Stokes equations. For a function f, its filtered form $\bar{f}$ and its Favre-averaged form $\tilde{f}$ are

$$\bar{f} = \frac{1}{V}\int_V Gf \,\mathrm{d}V, \qquad \tilde{f} = \frac{\overline{\rho f}}{\bar{\rho}}$$

where G is the filtering function and ρ is the density. From the Navier–Stokes equations for the instantaneous flow variables density ρ, velocity in the ith coordinate direction, u_i, pressure p, and temperature T, Favre-averaging and spatial filtering yield the filtered Navier–Stokes equations (here written using the Einstein summation notation, where repeated indices denote summation)

Received 3 December 1999; revision received 9 October 2000; accepted for publication 29 January 2001.

*Postdoctoral Associate, Department of Mechanical and Aerospace Engineering.

†Professor, Department of Mechanical and Aerospace Engineering. Associate Fellow AIAA.

$$\frac{\partial \bar{\rho}}{\partial t} + \frac{\partial \bar{\rho}\tilde{u}_k}{\partial x_k} = 0$$

$$\frac{\partial \bar{\rho}\tilde{u}_i}{\partial t} + \frac{\partial \bar{\rho}\tilde{u}_i\tilde{u}_k}{\partial x_k} = -\frac{\partial \bar{p}}{\partial x_i} + \frac{\partial \mathcal{T}_{ik}}{\partial x_k}$$

$$\frac{\partial \bar{\rho}\tilde{e}}{\partial t} + \frac{\partial}{\partial x_k}(\bar{\rho}\tilde{e} + \bar{p})\tilde{u}_k = \frac{\partial}{\partial x_k}(\mathcal{Q}_k + \mathcal{T}_{ik}\tilde{u}_i)$$

$$\bar{p} = \bar{\rho}R\tilde{T}$$

where

$$\mathcal{T}_{ik} = \tau_{ik} + \bar{\sigma}_{ik}, \qquad \mathcal{Q}_k = Q_k + \bar{q}_k$$

$$\tau_{ik} = -\bar{\rho}(\widetilde{u_i u_k} - \tilde{u}_i\tilde{u}_k), \qquad Q_k = -\bar{\rho}c_p(\widetilde{Tu_k} - \tilde{T}\tilde{u}_k)$$

$$\bar{\sigma}_{ik} = \mu(\tilde{T})\left(-\frac{2}{3}\frac{\partial \tilde{u}_j}{\partial \tilde{x}_j}\delta_{ik} + \frac{\partial \tilde{u}_i}{\partial x_k} + \frac{\partial \tilde{u}_k}{\partial x_i}\right), \qquad \bar{q}_k = k(\tilde{T})\frac{\partial \tilde{T}}{\partial x_k}$$

$$\bar{\rho}\tilde{k} = \frac{1}{2}(\overline{\rho u_i u_i} - \bar{\rho}\tilde{u}_i\tilde{u}_i) = -\frac{1}{2}\tau_{ii}$$

$$\bar{\rho}\tilde{e} = \bar{\rho}c_v\tilde{T} + \frac{1}{2}\bar{\rho}\tilde{u}_i\tilde{u}_i + \bar{\rho}\tilde{k}$$

Note that the specific form of the energy equation proposed by Knight et al.[5] was found by Martin et al.[26] to provide an accurate model of the SGS turbulent diffusion in decaying compressible isotropic turbulence. Two different SGS models are implemented in the LES code, and results are presented herein. The first is the classical constant-coefficient Smagorinsky model

$$\tilde{S}_{ij} = \frac{1}{2}\left(\frac{\partial \tilde{u}_i}{\partial \tilde{x}_j} + \frac{\partial \tilde{u}_j}{\partial \tilde{x}_i}\right)$$

$$\tau_{ij} = 2C_R\bar{\rho}\Delta^2\sqrt{\tilde{S}_{mn}\tilde{S}_{mn}}\left(\tilde{S}_{ij} - \frac{1}{3}\tilde{S}_{kk}\delta_{ij}\right)$$

$$Q_j = \bar{\rho}c_p\frac{C_R}{Pr_t}\Delta^2\sqrt{\tilde{S}_{mn}\tilde{S}_{mn}}\frac{\partial \tilde{T}}{\partial x_j}$$

where $C_R = 0.00423$ is the model coefficient, $Pr_t = 0.4$, and Δ is the length scale defined by[5]

$$\Delta = \left[\frac{1}{2}(V_l + V_r)\right]^{\frac{1}{3}} D$$

where V_l and V_r are the tetrahedral volumes to the left and right of the cell face and $D = 1 - e^{-n^+/26}$ is the Van Driest damping factor, where $n^+ = nu_\tau/\nu_w$ is the normal distance to the (nearest) solid boundary normalized by the viscous length scale ν_w/u_τ, ν_w is the kinematic viscosity evaluated at the wall, and u_τ is the local friction velocity.

The second model is MILES[7] wherein the inherent dissipation in the numerical algorithm is taken as the SGS model, that is, $C_R = 0$. The accuracy of MILES depends on the numerical algorithm. The theoretical basis of MILES is rigorously discussed by Fureby and Grinstein.[9] Excellent results have been obtained in numerous simulations of free shears flows.[7–11]

Numerical Method

We simplify the notation by hereafter dropping the tilde and overbar. Furthermore, the flow variables are nondimensionalized using the reference density ρ_∞, velocity U_∞, static temperature T_∞, and length scale L, with Mach number $M_\infty = U_\infty/\sqrt{(\gamma RT_\infty)}$. The governing equations may be written in finite volume form for a control volume V with surface ∂V:

$$\frac{\mathrm{d}}{\mathrm{d}t}\int_V Q\,\mathrm{d}V + \int_{\partial V}(F\hat{\imath} + G\hat{\jmath} + H\hat{k})\cdot\hat{n}\,\mathrm{d}A = 0$$

where

$$Q = \begin{Bmatrix}\rho\\ \rho u\\ \rho v\\ \rho w\\ \rho e\end{Bmatrix}, \qquad F = \begin{Bmatrix}\rho u\\ \rho u^2 + p - \mathcal{T}_{xx}\\ \rho uv - \mathcal{T}_{xy}\\ \rho uw - \mathcal{T}_{xz}\\ (\rho e + p)u - \mathcal{Q}_x - \beta_x\end{Bmatrix}$$

$$G = \begin{Bmatrix}\rho v\\ \rho uv - \mathcal{T}_{xy}\\ \rho v^2 + p - \mathcal{T}_{yy}\\ \rho vw - \mathcal{T}_{yz}\\ (\rho e + p)v - \mathcal{Q}_y - \beta_y\end{Bmatrix}$$

$$H = \begin{Bmatrix}\rho w\\ \rho uw - \mathcal{T}_{xz}\\ \rho vw - \mathcal{T}_{yz}\\ \rho w^2 + p - \mathcal{T}_{zz}\\ (\rho e + p)w - \mathcal{Q}_z - \beta_z\end{Bmatrix}$$

$$\beta_x = \mathcal{T}_{xx}u + \mathcal{T}_{xy}v + \mathcal{T}_{xz}w$$

$$\beta_y = \mathcal{T}_{xy}u + \mathcal{T}_{yy}v + \mathcal{T}_{yz}w$$

$$\beta_z = \mathcal{T}_{xz}u + \mathcal{T}_{yz}v + \mathcal{T}_{zz}w$$

An unstructured grid of tetrahedra is employed, with a cell-centered storage architecture. The cell-averaged values, stored at the centroid of each tetrahedron of volume V_i, are

$$Q_i = \frac{1}{V_i}\int_{V_i} Q\,\mathrm{d}V$$

The inviscid fluxes are computed using an exact one-dimensional Riemann solver [Godunov's method (see Ref. 27)] applied normal to each face. The inviscid flux computations require the values of each variable on either side of the cell faces. These values are obtained from the cell-averaged values by second-order or third-order function reconstruction using the least-squares method of Ollivier-Gooch.[28] More details on the reconstruction schemes are given by Okongo'o and Knight.[6] The viscous fluxes and heat transfer are computed by application of the Gauss theorem to the control volume whose vertices are the centroids of the cells that share each node. The second-order accurate scheme (in two dimensions) is given by Knight.[29]

Rescaling–Reintroducing Method

A compressible extension of the method of Lund et al.[12] has been developed. The simulation generates its own inflow conditions through a sequence of operations where the flowfield at a downstream station is rescaled and reintroduced at the inflow boundary (Fig. 1). The idea is to decompose each flowfield component into

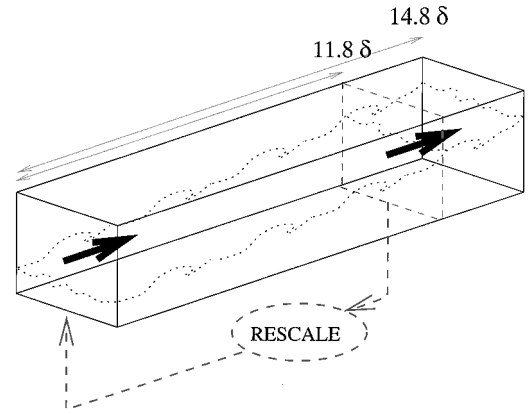

Fig. 1 Generation of inflow boundary condition.

a time mean and fluctuating part, and then to apply the appropriate scaling law to each one separately. Note that such a method can be used to generate the inflow database for a second computation such as a supersonic turbulent boundary layer past a compression corner.[30]

A variable $u(x, y, z, t)$ is decomposed into a time mean part $U(x, y, z)$ and an instantaneous time fluctuating part $u''(x, y, z, t)$ according to

$$U = \frac{1}{t_f - t_i}\int_{t_i}^{t_f} u\,\mathrm{d}t, \qquad u'' = u - U$$

As a compressible flow is considered, we note the Van Driest–Fernholz and Finley transformation of the velocity U as U_{VD}. In the case of an adiabatic flat plate flow

$$U_{\mathrm{VD}} = \frac{U_\infty}{A}\sin^{-1}\left(A\frac{U}{U_\infty}\right)$$

with

$$A = \sqrt{\frac{[(\gamma-1)/2]M_\infty^2 Pr_{t_m}}{1+[(\gamma-1)/2]M_\infty^2 Pr_{t_m}}}$$

where $Pr_{t_m} = 0.89$ is the mean turbulent Prandtl number.

The multilayer scaling is applicable for compressible and incompressible turbulent boundary layers.[31] Let us consider the inner region and the outer region of the boundary layer separately. On the inner side, a straightforward extension of the classical law of the wall reads in Van Driest coordinates

$$U_{\mathrm{VD}}^{\mathrm{inn}} = u_\tau(x) f_1(y^+) \qquad \text{with} \qquad f_1(y^+) = 1/\kappa\,\ell n(y^+) + C$$

where $y^+ = y u_\tau/\nu_w$ is the wall coordinate, u_τ is the mean friction velocity, ν_w is the kinematic viscosity evaluated at the wall, κ is von Kármán's constant, and C is a constant.

On the outer side, the defect law reads, also in Van Driest coordinates,

$$U_{\mathrm{VD}}^{\infty} - U_{\mathrm{VD}}^{\mathrm{out}} = u_\tau(x) f_2(\eta)$$

where $\eta = y/\delta$ is the outer coordinate, δ is the boundary-layer thickness, U_{VD}^{∞} is the free-stream value of the Van Driest transformed velocity, and f_2 is a second universal function (at this stage, there is no need to define it more precisely).

The functions f_1 and f_2 are independent of the streamwise position x. Consequently, the velocity U_{rec} at a suitable downstream station (recycle station) and the velocity U_{inl} at the inflow boundary (inlet station) can be related according to

$$U_{\mathrm{VD,inl}}^{\mathrm{inn}} = \beta U_{\mathrm{VD,rec}}\left(y_{\mathrm{inl}}^+\right)$$

in the inner region, and

$$U_{\mathrm{VD,inl}}^{\mathrm{out}} = \beta U_{\mathrm{VD,rec}}(\eta_{\mathrm{inl}}) + (1-\beta)U_{\mathrm{VD}}^{\infty}$$

in the outer region, where $\beta = u_{\tau,\mathrm{inl}}/u_{\tau,\mathrm{rec}}$ is the ratio of friction velocity between the inlet station and the recycled station. Notice that y_{inl}^+ and η_{inl} are the inner and outer coordinates at the inlet station, but $U_{\mathrm{VD,rec}}$ is evaluated at the recycle station.

The fluctuating part of the streamwise velocity is decomposed in a similar way. The velocity fluctuation in the inner and outer domains are rescaled according to

$$u_{\mathrm{inl}}^{\prime\prime\mathrm{inn}} = \beta u_{\mathrm{rec}}''\left(y_{\mathrm{inl}}^+, z, t\right), \qquad u_{\mathrm{inl}}^{\prime\prime\mathrm{out}} = \beta u_{\mathrm{rec}}''(\eta_{\mathrm{inl}}, z, t)$$

The scaling for the mean wall-normal velocity compound is assumed to be

$$V_{\mathrm{inl}}^{\mathrm{inn}} = V_{\mathrm{rec}}\left(y_{\mathrm{inl}}^+\right), \qquad V_{\mathrm{inl}}^{\mathrm{out}} = V_{\mathrm{rec}}(\eta_{\mathrm{inl}})$$

Notice that such a simple scaling is used as a convenient approximation that avoid computing the derivatives $\partial u_\tau/\partial x$ and $\partial\delta/\partial x$ needed to be consistent with the streamwise velocity scaling. Such approximation appears to be sufficient for a zero pressure gradient boundary layer.[32] The fluctuating wall-normal velocity v'' is scaled similarly to u''.

For the spanwise velocity compound, no scaling is needed because the mean value at the inflow boundary is set to zero. The w'' velocity fluctuation is scaled similarly to u''.

The temperature is scaled to take into account the compressibility effects as well. As the streamwise pressure gradient is negligible compared to the wall-normal temperature gradient, the following scaling is used for the mean temperature:

$$T_{\mathrm{inl}}^{\mathrm{inn}} = T_{\mathrm{rec}}\left(y_{\mathrm{inl}}^+\right), \qquad T_{\mathrm{inl}}^{\mathrm{out}} = T_{\mathrm{rec}}(\eta_{\mathrm{inl}})$$

In a supersonic boundary layer, the static pressure fluctuations are small compared to the temperature fluctuations.[33] We, therefore, assume

$$T_{\mathrm{inl}}^{\prime\prime\mathrm{inn}} = T_{\mathrm{rec}}''\left(y_{\mathrm{inl}}^+, z, t\right), \qquad T_{\mathrm{inl}}^{\prime\prime\mathrm{out}} = T_{\mathrm{rec}}''(\eta_{\mathrm{inl}}, z, t)$$

At this stage, the complete profiles for velocity and temperature valid over the entire inflow boundary layer are obtained by forming a weighted average of the inner and outer profile, as proposed by Lund et al.[12]:

$$u_{\mathrm{inl}} = \left(U_{\mathrm{inl}}^{\mathrm{inn}} + u_{\mathrm{inl}}^{\prime\prime\mathrm{inn}}\right)[1 - W(\eta_{\mathrm{inl}})] + \left(U_{\mathrm{inl}}^{\mathrm{out}} + u_{\mathrm{inl}}^{\prime\prime\mathrm{out}}\right)W(\eta_{\mathrm{inl}})$$

The weighting function W is defined as

$$W(\eta) = \frac{1}{2}\left(1 + \left\{\tanh\left[\frac{4(\eta - B)}{(1-2B)\eta + B}\right] \Big/ \tanh(4)\right\}\right)$$

using $B = 0.2$ to provide a smooth transition[12] at $y/\delta = 0.2$.

A similar weighted average is employed for the other two components of velocity and the static temperature. The static pressure is assumed constant at the inflow because the pressure fluctuations are small compared to the static temperature fluctuations.[33]

The last stage of the rescaling process consists in determining β and $\delta_{\mathrm{rec}}/\delta_{\mathrm{inl}}$. Best results have been obtained by imposing the ratio $u_{\tau,\mathrm{inl}}/u_{\tau,\mathrm{rec}}$ and $\delta_{\mathrm{inl}}/\delta_{\mathrm{rec}}$ according to the following classical empirical correlations[34]:

$$\frac{\delta_{\mathrm{rec}}}{\delta_{\mathrm{inl}}} = \left[1 + \left(\frac{x_{\mathrm{rec}} - x_{\mathrm{inl}}}{\delta_{\mathrm{inl}}}\right)0.27^{\frac{6}{5}} Re_{\delta_{\mathrm{inl}}}^{-\frac{1}{5}}\right]^{\frac{5}{6}}$$

$$\frac{u_{\tau,\mathrm{inl}}}{u_{\tau,\mathrm{rec}}} = \left(\frac{\delta_{\mathrm{rec}}}{\delta_{\mathrm{inl}}}\right)^{\frac{1}{10}} \tag{1}$$

where $Re_{\delta_{\mathrm{inl}}}$ is the Reynolds number based on the incoming boundary-layer thickness.

Configuration

A Mach 3 adiabatic flat plate turbulent boundary layer at Reynolds number $Re_\delta = 2\times10^4$ is simulated (where to simplify notation we employ δ for δ_{inl}). When x, y and z denote the streamwise, transverse, and spanwise directions, respectively, the computational domain is $L_x = 14.8\delta$, $L_y = 3.4\delta$, and $L_z = 1.1\delta$, 2.2δ, or 4.4δ. The spanwise width L_z ranges from approximately one to four times the experimental spanwise streak spacing (assuming the compressible turbulent boundary-layer streaks scale in accordance with incompressible experimental results[35]). The streamwise length L_x is approximately three times the mean experimental streamwise streak size. The height L_y is based on the requirement that acoustic disturbances originating at the upper boundary do not interact with the boundary layer on the lower wall. All computations employ $x_{\mathrm{rec}} - x_{\mathrm{inl}} = 11.8\delta$. The experimental data of Ünalmis and Dolling[36] indicates that the maximum cross-correlation coefficient of the surface pressure fluctuations in a Mach 5 turbulent boundary layer is approximately 0.1 at a distance of 10δ. Moreover, $x_{\mathrm{rec}} - x_{\mathrm{inl}}$ is approximately twice the mean experimental streamwise streak spacing of 1000 wall units.[35] Thus, the value of $x_{\mathrm{rec}} - x_{\mathrm{inl}}$ is considered sufficiently large to allow the turbulent structures to evolve independently of the recycle location. When Eq. (1), is used, $\delta_{\mathrm{rec}}/\delta_{\mathrm{inl}} = 1.27$ and $u_{\tau,\mathrm{inl}}/u_{\tau,\mathrm{rec}} = 1.03$. The different grid resolutions used are shown

Table 1 Details of grids

	At the wall			At $y = \delta$				
Name	Δx^+	Δy^+	Δz^+	$\Delta x/\delta$	$\Delta y/\delta$	$\Delta z/\delta$	L_z/δ	Tetras
Baseline Smagorinsky	11	1.1	3.1	0.09	0.105	0.069	1.1	1,688,960
Baseline MILES	11	1.1	3.1	0.09	0.105	0.069	1.1	1,688,960
Singlewidth MILES	18	1.5	6.5	0.10	0.140	0.034	1.1	816,000
Doublewidth MILES	18	1.5	6.5	0.10	0.140	0.034	2.2	1,632,000
Quadruplewidth MILES	18	1.5	6.5	0.10	0.140	0.034	4.4	3,264,000
Coarse Smagorinsky	28	0.9	13	0.15	0.086	0.069	4.4	320,000
Coarse MILES	28	0.9	13	0.15	0.086	0.069	4.4	320,000
Xverycoarse MILES	56	0.9	13	0.30	0.086	0.069	4.4	160,000
Yverycoarse MILES	28	1.7	13	0.15	0.165	0.069	4.4	166,400
Zverycoarse MILES	28	0.9	26	0.15	0.086	0.137	4.4	160,000

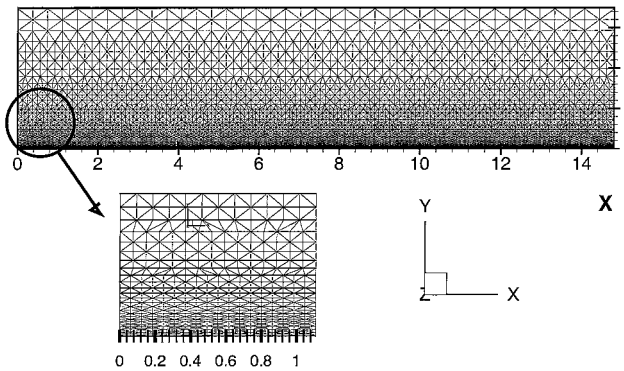

Fig. 2 Computational mesh (baseline Smagorinsky).

in Table 1, and an example is shown in Fig. 2. The height Δy^+ of the first cell adjacent to the boundary is approximately one wall unit [$\Delta y \approx \nu_w/u_\tau$, where ν_w is the kinematic viscosity at the wall, $u_\tau = \sqrt{(\tau_w/\rho_w)}$ is the friction velocity, τ_w is the wall shear stress, and ρ_w is the density at the wall].

The initial condition for the coarse Smagorinsky computation (Table 1) is a turbulent mean profile with random fluctuations. The simulation is run first for 135 inertial timescales δ/U_∞ to eliminate starting transients.[12] At this stage, the flow is used as an initial condition for all other computations. Such a technique assures an adequate flowfield initialization that minimizes the transient period.

For comparison with experiment, the primitive variables are averaged both in time and in the spanwise (homogeneous) direction. The time period is $t_f - t_i = 40\delta/U_\infty$. The notation for the combined temporal and spanwise average of a function $f(x, y, z, t)$ is

$$\langle\langle f \rangle\rangle = \frac{1}{L_z}\frac{1}{t_f - t_i}\int_0^{L_z}\int_{t_i}^{t_f} f \, \mathrm{d}t \, \mathrm{d}z$$

SGS Model Influence

LES studies were performed for two different grids (baseline and coarse in Table 1) using the Smagorinsky and MILES models to assess the effect of including the Smagorinsky model. In the baseline case, the grid in the near-wall region is comparable to a DNS grid with $\Delta x^+ = 11$, $\Delta y^+ = 1.1$, and $\Delta z^+ = 3.1$. The grid is stretched in all three directions away from the wall (see Fig. 2), and the grid spacing near the edge of the boundary layer is substantially larger than would be used for DNS. In the coarse case, the grid in the x and z directions near the wall is increased by a factor of 2.55 and 4.19, respectively, compared to the baseline grid. The grid spacing in the x and y directions near the edge of the boundary layer is changed by a factor of 1.67 and 0.82 relative to the baseline grid, and the grid spacing in the z direction is the same as employed for the baseline grid.

The friction velocity predicted by the coarse MILES, $u_\tau/U_\infty = 0.0528$, is within 1% of the coarse Smagorinsky, $u_\tau/U_\infty = 0.0532$. Similarly, the friction velocity predicted by the baseline MILES, $u_\tau/U_\infty = 0.0560$, is within 1% of the baseline Smagorinsky, $u_\tau/U_\infty = 0.0556$. The streamwise mean velocity profiles using the coarse grid are plotted in Fig. 3. The two profiles are virtually identical. The same trend is observed by comparing the

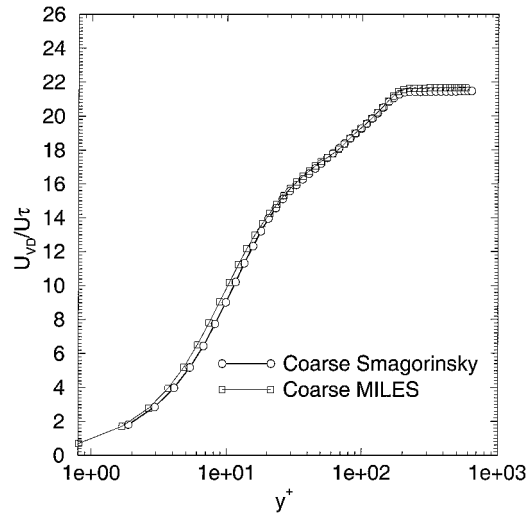

Fig. 3 Mean streamwise velocity.

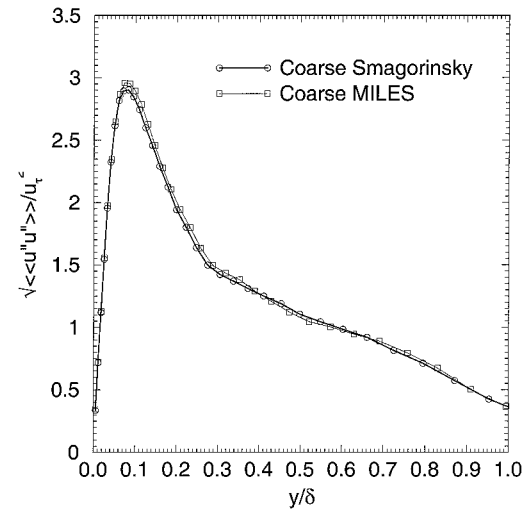

Fig. 4 Streamwise Reynolds stress.

streamwise and wall-normal velocity fluctuations (Figs. 4 and 5). Similar results are obtained using the baseline grids. Additionally, the local turbulent viscosity predicted by the Smagorinsky model never exceeds 27% of the molecular viscosity. We conclude that inclusion of the Smagorinsky model has a negligible effect on the turbulence statistics. Consequently, the remaining results were obtained using MILES.

Grid Refinement

A series of LES studies were performed using the MILES model to assess the effect of grid refinement on the flowfield (Table 1). The baseline grid has the finest mesh in general (except for Δz in

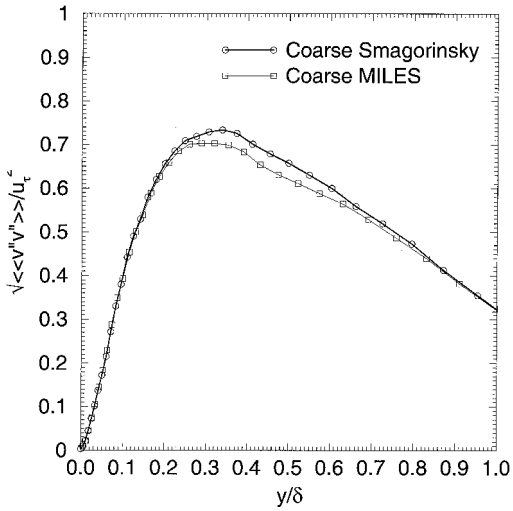

Fig. 5 Wall normal Reynolds stress.

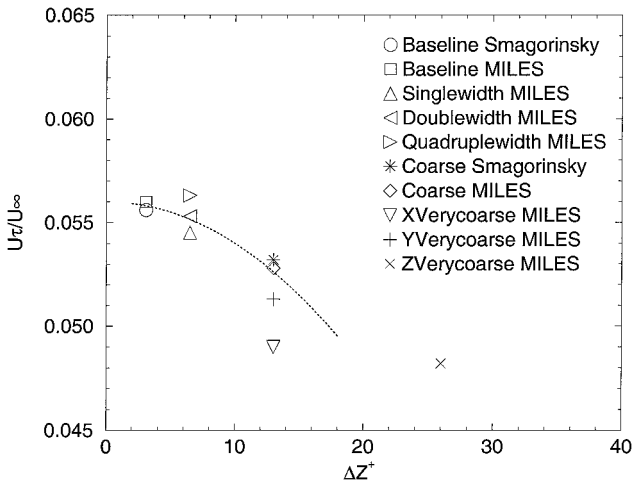

Fig. 6 Effect of Δz_w^+ on friction velocity.

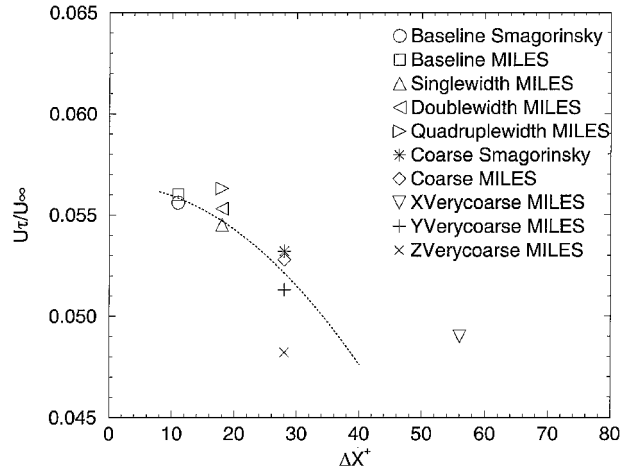

Fig. 7 Effect of Δx_w^+ on friction velocity.

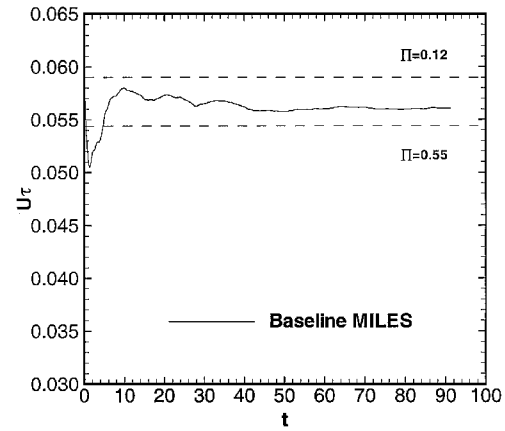

Fig. 8 Temporal evolution of u_τ (baseline MILES).

the outer portion of the boundary layer). The baseline grid spacing near the wall was selected to resolve fully the sublayer streaks based on classical incompressible turbulent boundary-layer scaling laws.[35] Two sets of grids were considered in addition to the baseline grid. The first set (singlewidth, doublewidth, and quadruplewidth) employed identical grid distributions with spanwise domain sizes $L_z = 1.1\delta$, 2.2δ, and 4.4δ, respectively. Compared to the baseline case, the grid spacing near the wall was increased by factors of 1.64, 1.36, and 2.1 in the x, y, and z directions, respectively. The purpose of the first set is to evaluate the effect of the near-wall grid spacing and spanwise domain size L_z on the flowfield. The second set (coarse, Xverycoarse, Yverycoarse and Zverycoarse) represented a successive doubling of the grid spacing in the x, y, and z directions relative to the coarse case, which itself employed a larger grid spacing than the baseline. The purpose of the second set is to evaluate the effect of the grid spacing in the x, y, and z directions on the flowfield.

The computed friction velocity u_τ / U_∞ is presented in Figs. 6 and 7 vs Δz^+ and Δx^+, respectively. There is negligible practical difference (less than 3%) between the baseline, singlewidth, doublewidth, and quadruplewidth results. There is a significant difference (up to 15% underprediction) between the baseline and the Xverycoarse, Yverycoarse, and Zverycoarse grids. This implies that the latter grids are too coarse because previous studies have shown that underresolved LES of a turbulent boundary layer underestimates the friction velocity.[16] The coarse grid result is within 6% of the baseline grid. We may, therefore, conclude the following with regards to the effect of the grid spacing on u_τ. First, the grid resolution afforded by the singlewidth case (which is the same as the doublewidth and quadruplewidth) is adequate for LES of the supersonic boundary layer, that is, $\Delta x^+ = 18$, $\Delta y^+ = 1.5$, and $\Delta z^+ = 6.5$ at the wall and $\Delta x \approx \Delta y \approx \Delta z \approx 0.1\delta$ near the edge of the boundary layer. Second, there is a very small effect of L_z on u_τ for $1.1\delta \leq L_z \leq 4.4\delta$.

Note that our LES studies use a coarser grid overall than required for DNS. For example, we may compare the singlewidth grid with the DNS grid of Adams[37] for the same Mach number and comparable Reynolds number. At the wall, $\Delta x^+_{\text{LES}} \approx 3.3\ \Delta x^+_{\text{DNS}}$, $\Delta y^+_{\text{LES}} \approx 1.5 \Delta y^+_{\text{DNS}}$, and $\Delta z^+_{\text{LES}} \approx 3.1\ \Delta z^+_{\text{DNS}}$, and at the edge of the boundary layer, $\Delta x_{\text{LES}} > 3\ \Delta x_{\text{DNS}}$, $\Delta y_{\text{LES}} > 4\ \Delta y_{\text{DNS}}$, and $\Delta z_{\text{LES}} > 6\ \Delta z_{\text{DNS}}$.

Comparison of MILES Results with Experiments

The theoretical value of the friction velocity u_τ for a supersonic adiabatic flat plate boundary layer is obtained from the combined law of the wall and wake evaluated at $y = \delta$:

$$1/\kappa\ \ell n(y u_\tau / \nu_w) + C + (2\Pi/\kappa) = (U_\infty / A u_\tau) \sin^{-1} A$$

where $\kappa = 0.40$ is von Kármán's constant and $C = 5.1$. The wake parameter Π depends on the Reynolds number (see Ref. 31). For high Reynolds numbers, $\Pi = 0.55$, whereas at $Re_\delta = 2 \times 10^4$ an extrapolation of the available experimental data indicates $\Pi \approx 0.12$. The corresponding values of u_τ / U_∞ are 0.054 and 0.059. The uncertainty in the experimental data of skin friction is typically $\pm 5\%$ as discussed by Hopkins and Inouye.[38] The LES prediction reaches a steady value $u_\tau / U_\infty = 0.056$ after 38,400 time steps (Fig. 8), which is within the two limiting values.

The computed adiabatic wall temperature is $T_{\text{aw}} / T_\infty = 2.66$, which is within 3% of the theoretical value of 2.602 obtained from the empirical formula[39]

$$T_{\text{aw}} / T_\infty = 1 + [(\gamma - 1)/2] Pr_{t_m} M_\infty^2$$

where $Pr_{t_m} = 0.89$ is the mean turbulent Prandtl number.

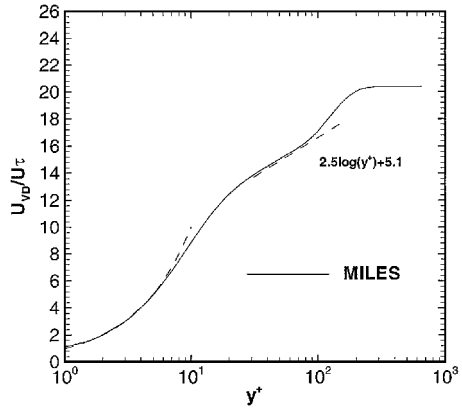

Fig. 9 Mean streamwise velocity (baseline MILES).

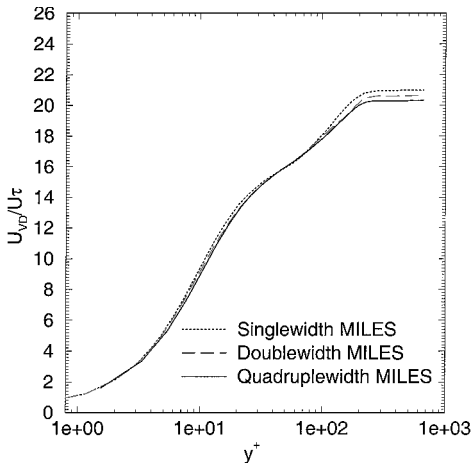

Fig. 10 Mean streamwise velocity for three different L_z.

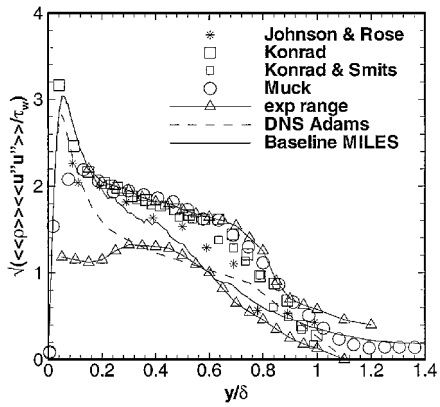

Fig. 11 Streamwise Reynolds stress.

The mean streamwise velocity profile using the Van Driest transformation is shown in Fig. 9. The viscous sublayer approximation $U_{\mathrm{VD}}/u_\tau = y^+$ and Law of the Wall $U_{\mathrm{VD}}/u_\tau = \kappa^{-1}\log(y^+) + C$ are drawn for comparison. The computed profile using MILES is in excellent agreement with the law of the wall with a logarithmic region appearing clearly in the range $30 < y^+ < 150$.

The effect of the spanwise domain size L_z on the mean velocity profile is shown in Fig. 10, where the computed profiles for singlewidth, doublewidth, and quadruplewidth grids are shown. These three configurations differ only by the spanwise length of the simulation domain. The singlewidth domain displays the strongest wake effect, whereas the doublewidth and quadruplewidth domains show virtually identical velocity profiles. We conclude that the doublewidth case ($L_z = 2.2\delta$) has an adequate spanwise domain size for the configuration examined that is, for $L_x = 14.8\delta$.

As discussed in Zheltovodov and Yakovlev[40] and Smits and Dussauge,[34] the scalings $\langle\langle\rho\rangle\rangle\langle\langle u''u''\rangle\rangle/\tau_w$ and $\langle\langle\rho\rangle\rangle\langle\langle u''v''\rangle\rangle/\tau_w$ provide an approximate self-similar correlation of experimental data for supersonic flat plate zero pressure gradient adiabatic boundary layers, although the measurements close to the wall are subject to considerable uncertainty. Figure 11 displays the computed results using the baseline grid together with the experimental data of Konrad and Smits,[41] Johnson and Rose,[42] Muck et al.,[43] and Konrad,[44] as well as upper and lower bounds of an extensive set of experimental data for the Mach number range $M = 1.72-9.4$ compiled by Zheltovodov and Yakovlev.[40] The characteristics of the different experiments are shown in Table 2. The computed results show good agreement with experiment for the main part of the boundary layer ($y/\delta > 0.2$), despite significantly higher experimental Reynolds numbers. For $y/\delta < 0.2$, the presence of the typical high-level peak in the near-wall region is supported by experimental data of Konrad,[44] and the DNS data of Adams[37] (see also Fig. 12), which is at nearly the same Reynolds number as the LES. However, no conclusion can be drawn regarding the location of the peak without further experimental data or DNS. Similar close ageement is observed for the Reynolds shear stress distributions (Figs. 13 and 14).

An instantaneous image of the vorticity modulus at $y^+ = 25$ is shown in Fig. 15. The hairpin vortices are clearly evident in agreement with experiment and DNS.[35]

Table 2 Flow parameters[a]

Name	Mach no.	$Re_\delta \times 10^3$
LES (Smagorinsky, MILES)	3.0	20
DNS Adams[37]	3.0	25
Johnson and Rose[42]	2.9	1000
Konrad[44]	2.9	1590
Konrad and Smits[41]	2.87	1900
Muck et al.[43]	2.87	1638
Zheltovodov and Yakovlev[40]	1.7–9.4	≤2000

[a]All cases with adiabatic wall.

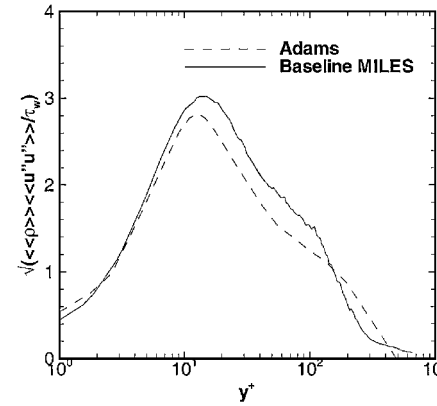

Fig. 12 Streamwise Reynolds stress.

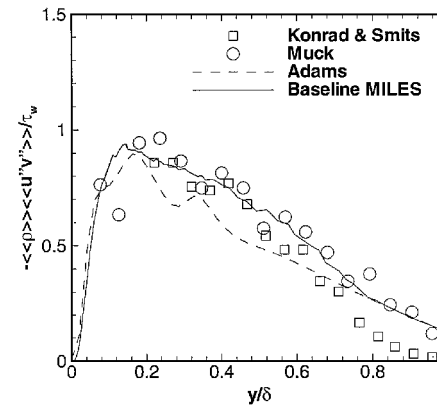

Fig. 13 Reynolds shear stress.

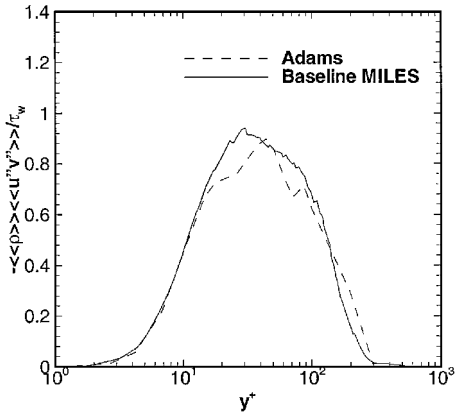

Fig. 14 Reynolds shear stress.

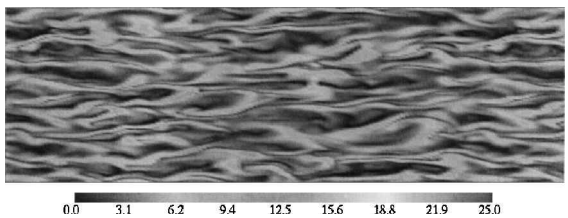

Fig. 15 Modulus of vorticity at $y^+ = 25$ (coarse Smagorinsky).

Conclusions

A three-dimensional fully unstructured grid LES algorithm for compressible turbulent flow has been presented. The algorithm is second- or third-order accurate in space and second-order accurate in time. The algorithm is applied to the LES of a supersonic adiabatic flat plate boundary layer at Mach 3 and $Re_\delta = 2 \times 10^4$. A compressible extension of the rescaling–reintroducing process of Lund et al.[12] has been developed to generate the inflow conditions. Comparisons of the MILES and Smagorinsky models indicate virtually identical results, implying that the Smagorinsky model is not needed for this flow. A detailed grid refinement study is presented, and criteria are established for effectively grid independent results. The computed flowfield is in good agreement with experimental data for friction velocity, adiabatic wall temperature, mean velocity, and Reynolds stresses.

Acknowledgments

This research is supported by the Air Force Office of Scientific Research under Grant F49620-99-1-0008 monitored by L. Sakell. The computations were performed at Rutgers University and the National Center for Supercomputing Applications and the Scientific Computing Facility Boston University under Grant CTS980016N. The authors express appreciation to A. Zheltovodov for helpful discussions and information.

References

[1]Lesieur, M., and Metais, O., "New Trends in Large-Eddy Simulations of Turbulence," *Annual Review of Fluid Dynamics*, Vol. 28, 1996, pp. 45–82.

[2]Ferziger, J., "Large Eddy Simulation: An Introduction and Perspective," *New Tools in Turbulence Modeling*, Springer-Verlag, Berlin, 1996, pp 29–47.

[3]Sagaut, P., and Lê, T., and Moschetti, P., "LES-DNS: The Aeronautical and Defense Point of View," *New Tools in Turbulence Modeling,* Springer-Verlag, Berlin, 1996, pp. 183–197.

[4]Thompson, J., and Soni, B., and Weatherill, N., *Handbook of Grid Generation*, CRC Press, Boca Raton, FL, 1999, Chap. 16.

[5]Knight, D., Zhou, G., Okong'o, N., and Shukla, V., "Compressible Large Eddy Simulation Using Unstructured Grids," AIAA Paper 98-0535, Jan. 1998.

[6]Okong'o, N., and Knight, D., "Compressible Large Eddy Simulation Using Unstructured Grids: Channel and Boundary Layer Flows," AIAA Paper 98-3315, July 1998.

[7]Boris, J., Grinstein, F., Oran, E., and Kolbe, R., "New Insights into Large Eddy Simulation," *Fluid Dynamics Research*, Vol. 10, 1992, pp. 199–228.

[8]Oran, E., and Boris, J., "Computing Turbulent Shear Flows–A Convenient Conspiracy," *Computers in Physics*, Vol. 7, No. 5, 1993, pp. 523–533.

[9]Fureby, C., and Grinstein, F., "Monotically Integrated Large Eddy Simulation of Free Shear Flows," *AIAA Journal*, Vol.37, No. 5, 1999, pp. 544–556.

[10]Grinstein, F., "Dynamics of Coherent Structures and Transition to Turbulence in Free Square Jets," AIAA Paper 96-0781, Jan. 1996.

[11]Porter, D., Pouquet, A., and Woodward, P., "Kolmogorov-Like Spectra in Decaying Three-Dimensional Supersonic Flows," *Physics of Fluids*, Vol. 6, No. 6, 1994, pp. 2133–2142.

[12]Lund, T., Wu, X., and Squires, K., "Generation of Turbulent Inflow Data for Spatially-Developing Boundary Layer Simulations," *Journal of Computational Physics*, Vol. 140, No. 2, 1998, pp. 233–258.

[13]Erlebacher, G., Hussaini, M., Speziale, C., and Zang, T., "Toward the Large-Eddy Simulation of Compressible Turbulent Flows," *Journal of Fluid Mechanics*, Vol. 238, May 1992, pp. 155–185.

[14]Spyropoulos, E., and Blaisdell, G., "Evaluation of the Dynamic Model for Simulations of Compressible Decaying Isotropic Turbulence," *AIAA Journal*, Vol. 34, No. 5, 1996, pp. 990–998.

[15]Jansen, K., "Large Eddy Simulation Using Unstructured Grids," *Advances in DNS/LES*, Greyden, Columbus, OH, 1997, pp. 117–128.

[16]Ducros, F., Comte, P., and Lesieur, M., "Large Eddy Simulation of Transition to Turbulence in a Boundary Layer Developing Spatially over a Flat Plate," *Journal of Fluid Mechanics*, Vol. 326, Nov. 1996, pp. 1–36.

[17]Haworth, D., and Jansen, K., "LES on Unstructured Deforming Meshes: Towards Reciprocating IC Engines," *Proceedings of the 1996 Summer Program, Center for Turbulence Research*, Stanford Univ./NASA Ames Research Center, 1996, pp. 329–346.

[18]Fasel, H., and Konzelmann, U., "Non-Parallel Stability of a Flat-Plate Boundary Layer Using the Complete Navier–Stokes Equations," *Journal of Fluid Mechanics*, Vol. 221, Dec. 1990, pp. 311–347.

[19]Joslin, R., Street, C., and Chang, C., "Spatial Direct Numerical Simulation of Boundary Layer Transition Mechanism: Validation of PSE Theory," *Theoretical and Computational Fluid Dynamics*, Vol. 4, No. 5, 1993, pp. 271–288.

[20]Kleiser, L., and Zang, T., "Numerical Simulation of Transition in Wall-Bounded Shear Flows," *Annual Review of Fluid Dynamics*, Vol. 23, 1991, pp. 495–537.

[21]Guo, Y., Adams, N., and Kleisler, L., "Modeling of Non-Parallel Effects in Temporal Direct Numerical Simulation of Compressible Boundary Layer," *Theoretical and Computational Fluid Dynamics*, Vol. 7, No. 2, 1995, pp. 141–157.

[22]Le, H., Moin, P., and Kim, J., "Direct Numerical Simulation of Turbulent Flow over a Backward Facing Step," *Journal of Fluid Mechanics*, Vol. 330, Jan. 1997, pp. 349–374.

[23]Spalart, P., and Yang, K., "Numerical Study of Ribbon-Induced Transition in Blasius Flow," *Journal of Fluid Mechanics*, Vol. 178, May 1987, pp. 345–365.

[24]Spalart, P., "Direct Simulation of a Turbulent Boundary Layer up to $R_\theta = 1410$," *Journal of Fluid Mechanics*, Vol. 187, Feb. 1988, pp. 61–98.

[25]El-Hady, N., Zang, T., and Piomelli, U., "Applications of the Dynamic Subgrid-Scale Model to Axisymmetric Transitional Boundary Layer at High Speed," *Physics of Fluids*, Vol. 6, No. 3, 1994, pp. 1299–1309.

[26]Martin, M., Piomelli, U., and Candler, G., "A Priori Tests of SGS Models in Compressible Turbulence," Third American Society of Mechanical Engineers/Japan Society of Mechanical Engineers, Joint Fluids Engineering Conf., July 1999.

[27]Gottlieb, J., and Groth, C., "Assessment of Riemann Solvers for Unsteady One-Dimensional Inviscid Flows of Perfect Gases," *Journal of Computational Physics*, Vol. 78, No. 2, 1988, pp. 437–458.

[28]Ollivier-Gooch, C., "High Order ENO Schemes for Unstructured Meshes Based on Least Squares Reconstruction," AIAA Paper 97-0540, Jan. 1997.

[29]Knight, D., "A Fully Implicit Navier–Stokes Algorithm Using an Unstructured Grid and Flux Difference Splitting," *Applied Numerical Mathematics*, Vol. 16, 1994, pp. 101–128.

[30]Urbin, G., Knight, D., and Zheltovodov, A., "Compressible Large Eddy Simulation Using Unstructured Grid: Supersonic Turbulent Boundary Layer and Compression Corner," AIAA Paper 99-0427, Jan. 1999.

[31]Fernholz, H., and Finley, P., "A Critical Commentary on Mean Flow Data for Two-Dimensional Compressible Turbulent Boundary Layers," Tech. Rept. 253, AGARD, May 1980.

[32]Arad, E., and Wolfshtein, M., "Analysis of Equilibrium Adverse Pressure Gradient Boundary Layer Using Large Eddy Simulation," AIAA Paper 99-0420, Jan. 1999.

[33]Kistler, A., and Chen, W., "A Fluctuating Pressure Field in a Supersonic Turbulent Boundary Layer," *Journal of Fluid Mechanics*, Vol. 16, May 1963, pp. 41–64.

[34]Smits, A., and Dussauge, J.-P., *Turbulent Shear Layers in Supersonic Flow*, American Inst. of Physics, New York, 1996, Chap. 2.

[35]Cantwell, B., "Organized Motion in Turbulent Flow," *Annual Review of Fluid Dynamics*, Vol. 13, 1981, pp.457–515.

[36]Unalmis, O., and Dolling, D., "Decay of Fluctuating Wall-Pressure Field of Mach 5 Turbulent Boundary Layer," *AIAA Journal*, Vol. 37, No. 9, 1999, pp. 1088–1096.

[37]Adams, N., "Direct Numerical Simulation of Turbulent Supersonic Boundary Layer Flow," *Advances in DNS/LES*, Greyden, Columbus, OH, 1997, pp. 29–40.

[38]Hopkins, E., and Inouye, M., "An Evaluation of Theories for Predicting Skin Friction and Heat Transfer on Flat Plates at Supersonic and Hypersonic Mach Numbers," *AIAA Journal*, Vol. 9, No. 6, 1971, pp. 993–1003.

[39]White, F., *Viscous Fluid Flow*, McGraw–Hill, New York, 1974, Chap. 7.

[40]Zheltovodov, A., and Yakovlev, V., "Stages of Development, Gas Dynamic Structure and Turbulence Characteristics of Turbulent Compressible Separated Flows in the Vicinity of 2-D Obstacles," Preprint 27-86, Inst. of Theoretical and Applied Mechanics, USSR Academy of Sciences, Novosibirsk, Russia, 1986 (in Russian).

[41]Konrad, W., and Smits, W., "Turbulence Measurements in a Three-Dimensional Boundary Layer in Supersonic Flow," *Journal of Fluid Mechanics,* Vol. 372, Oct. 1998, pp. 1–23.

[42]Johnson, D., and Rose, W., "Laser Velocimeter and Hot Wire Anemometer Comparison in a Supersonic Boundary Layer," *AIAA Journal*, Vol. 13, No. 4, 1975, pp. 512–515.

[43]Muck, K., Spina, E., and Smits, A., "Compilation of Turbulence Data for an 8 degree Compression Corner at Mach 2.9," Tech. Rept. MAE-1642, Princeton Univ., Princeton, NJ, April 1984.

[44]Konrad, W., "A Three Dimensional Supersonic Turbulent Boundary Layer Generated by an Isentropic Compression," Ph.D. Dissertation, Dept. Mechanical and Aerospace Engineering, Princeton Univ., Princeton, NJ, 1993.

J. Kallinderis
Associate Editor